Energy & Environmental Science

Realization of higher thermoelectric performance by dynamic doping of copper in n-type PbTe

Journal:	*Energy & Environmental Science*
Manuscript ID	EE-ART-04-2019-001137.R2
Article Type:	Paper
Date Submitted by the Author:	15-Aug-2019
Complete List of Authors:	You, Li; Shanghai University, School of Materials Science and Engineering Zhang, Jiye; Department of Electronic Information Materials, School of Materials Science and Engineering, Pan, Shanshan; b. School of Materials Science and Engineering, Shanghai University Jiang, Ying; Shanghai University, Materials Genome Institute Wang, Ke; Shanghai University, Materials Genome Institute Yang, Jiong; Shanghai University, Materials Genome Institute Pei, Yanzhong; Tongji University, Materials Science Zhu, Qing; University of Houston Agne, Matthias; Northwestern University, Materials Science Snyder, G.; Northwestern University, Materials Science Ren, Zhifeng; University of Houston, Department of Physics Zhang, Wenqing; Southern University of Science and Technology, Department of Physics Luo, Jun; Shanghai University, School of Materials Science and Engineering

Broader context

Optimizing electrical-transport properties over a wide temperature range is an intriguing and challenging issue in thermoelectrics, which directly relates to the output power density of a thermoelectric material. For a conventional doping method, electrical-transport properties can only be optimized for a given temperature because the achieved carrier concentration is a constant and do not change with varying temperature. To address this issue, a concept of "dynamic doping" was recently proposed to realize a temperature-dependent doping effect. However, it does not mean that the optimal electrical transport properties can be realized by simply dynamic doping. In fact, we find that the interstitial size should be controlled to realize the perfect dynamic doping effect. Thus, in this work, we propose the concept of 'interstitial engineering', which seems to be the sum of 'dynamic doping' and 'interstitial size manipulating'. Along the direction of "interstitial engineering", a prominent dynamic doping effect is achieved in n-type PbTe. As a result, the carrier concentration of PbTe can be fully optimized over a wide temperature range without significant deterioration of carrier mobility. A peak zT of ~1.3 and a calculated leg efficiency of 12% were achieved for the sample with 0.2 at% Cu. More importantly, with the reinforcement of "interstitial engineering", "dynamic doping" can be synergistically used with other sophisticated approaches, which may inspire new thinking in the doping design space for thermoelectrics.

Journal Name

ARTICLE

Realization of higher thermoelectric performance by dynamic doping of copper in n-type PbTe

Li You,‡[a,b] Jiye Zhang,‡[a] Shanshan Pan,[a] Ying Jiang,[c] Ke Wang,[c] Jiong Yang,[c] Yanzhong Pei,[d] Qing Zhu,[b] Matthias T. Agne,[e] G. Jeffrey Snyder,[e] Zhifeng Ren,*[b] Wenqing Zhang,*[f] and Jun Luo*[a,c]

Received 00th January 20xx,
Accepted 00th January 20xx

DOI: 10.1039/x0xx00000x

www.rsc.org/

It is a great challenge to optimize a material's thermoelectric performance due to the strong correlation between its thermoelectric-transport properties, especially the electrical-transport properties. Optimizing the peak *zT* using a constant carrier concentration is commonly adopted because of the difficulty in realizing the optimum temperature-dependent carrier concentration, but this is not meaningful for real applications, in which the average *zT* value over the working temperature range is much more important. Here we propose an effective strategy involving the dynamic doping effect of interstitial Cu atoms to fully optimize the electrical-transport properties of n-type PbTe over a wide temperature range. By using Cu intercalation, the temperature-dependent carrier concentration of PbTe is found to well match the theoretically optimal profile. Furthermore, high carrier mobility is largely maintained because the dynamic behavior of the interstitial Cu does not alter the band structure and therefore change the effective mass. Consequently, a peak *zT* of ~1.3 and a calculated leg efficiency of 12% were achieved for the sample with 0.2 at% Cu. Based on our findings, we further proposed a concept of 'interstitial engineering' to reinforce the dynamic doping effect, which is of fundamental importance for optimizing the thermoelectric properties.

Introduction

The thermoelectric performance of a material is determined jointly by its electrical- and thermal-transport properties. The electrical-transport performance is integrally reflected by the so-called thermoelectric power factor (*PF*), $PF = \sigma S^2$, where σ and S are the electrical conductivity and Seebeck coefficient, respectively. The thermal-transport properties are determined by the thermal conductivity κ, which is composed of electronic (κ_E) and lattice (κ_L) components. Thus, the dimensionless thermoelectric figure of merit zT, $zT = S^2\sigma T/\kappa$ (T is the absolute temperature), is commonly used to express the thermoelectric performance of a material.[1,2] In order to optimize the thermoelectric properties, it is clear that the power factor should be increased while the thermal conductivity should be decreased.

The electronic thermal conductivity relies on the electrical properties through $\kappa_E = L\sigma T$, where L is the Lorenz number, and cannot be manipulated independently.[3] On the other hand, significant achievements have been made in reducing the lattice thermal conductivity by enhancing phonon scattering.[4-9] Various approaches aiming to scatter heat-carrying phonons with different wavelengths have been adopted to reduce κ_L, such as introducing 0D point defects (including substitutional atoms,[10] interstitial atoms,[11] and vacancies[12,13]), 1D dislocations[12] and 2D grain boundaries,[9] or nano-sized precipitates[6] into the host material. In particular, maximum reduction of κ_L has been realized in the lead chalcogenides with all-scale hierarchical architectures.[7,8,14,15]

Unfortunately, optimization of the power factor is difficult, especially considering its temperature-dependent features. Both σ and S are closely correlated to the carrier-transport parameters (carrier concentration and mobility) and the band structure,[3] and all of these parameters change with the temperature.[16] Up to now, reports of the realization of optimal electrical-transport performance over the working temperature range remain rare, which could be ascribed to the following two reasons. 1) The optimum carrier concentration is not invariable, but is temperature-dependent, roughly following the relationship of $n_{opt} \sim (m^*T)^{1.5}$, where m^* is the density of states

[a] School of Materials Science and Engineering, Shanghai University, 99 Shangda Road, Shanghai 200444, China. E-mail: junluo@shu.edu.cn
[b] Department of Physics and Texas Center for Superconductivity University of Houston, Houston, TX 77204, USA. E-mail: zren@uh.edu
[c] Materials Genome Institute, Shanghai University, 99 Shangda Road, Shanghai 200444, China.
[d] School of Materials Science and Engineering, Tongji University, 4800 Caoan Road, Shanghai 201804, China.
[e] Department of Materials Science and Engineering, Northwestern University, Evanston, IL 60208, USA.
[f] Institute for Quantum Science and Engineering, Department of Physics, Southern University of Science and Technology, Shenzhen 518055, China. E-mail: zhangwq@sustc.edu.cn

† Electronic Supplementary Information (ESI) available: Some calculation details; Supplementary Note 1~4; Phase identification and microstructure analysis (Fig. S1-S2); Calculated tetrahedral interstitial space in lead chalcogenides (Fig. S3); Temperature dependence of carrier mobility and effective mass. (Fig. S4); Electronic band structures at 800K for PbTe and $PbCu_{0.01}Te$ (Fig. S5); Repeated measurement of thermoelectric properties (Fig. S6-S7).; Seebeck coefficient mapping of the $PbTeCu_{0.002}$ sample after 4 cycling measurements (Fig. S8). Room temperature Vickers hardness for Cu-free sample and 0.2 at% Cu doped PbTe sample (Fig. S9). Thermoelectric properties of $PbCu_xTe$ (x=0.05 and 0.1) (Fig. S10); Calculated carrier concentration-dependent power factors and figure of merit zT. (Fig. S11). See DOI: 10.1039/x0xx00000x

‡ These authors contributed equally to this work.

(DOS) effective mass.[16] In fact, the optimum carrier concentration at high temperature could be several times larger than that at room temperature. For the traditional doping method, the content of the extrinsic dopant is usually fixed, which always results in a constant carrier concentration, and, consequently, the best electrical properties are exhibited only at a given temperature.[17] 2) The traditional doping method usually leads to reduced carrier mobility and decreased electrical conductivity due to the carrier-scattering effect of the doped dissimilar atoms.[18] Therefore, it is essential to develop a novel strategy that can be used to optimize the electrical-transport properties over a wide temperature range.

In our previous work, we proposed the concept of dynamic doping.[19] This novel concept may open a new route to improve electrical transport properties over a wide temperature range. However, the dynamic doping effect in Cu-intercalated PbSe is not so distinct and predominant, indicating that the optimal electrical transport properties cannot be realized by simply dynamic doping. After a thorough investigation on the crystal structure of lead chalcogenides, we have realized that the interstitial space of the anion sublattice should be a determine factor for the degree of dynamic doping phenomenon. Therefore, a concept of 'interstitial engineering' is proposed in this work, which seems to be a synergy of 'dynamic doping' and 'interstitial size manipulating'. Along the direction of 'interstitial engineering', we have observed a nearly perfect dynamic doping phenomenon in the PbTe:Cu system, especially in the low temperature range. Besides, the Cu-intercalated PbTe shows a relatively high carrier mobility because neither the band structure nor the carrier-scattering mechanism is changed by the dynamic behavior of the interstitial Cu. Therefore, optimum temperature-dependent electrical-transport properties are realized in the n-type Cu-intercalated PbTe. Consequently, a satisfactory peak zT of ~1.3 and an excellent conversion leg efficiency ~12% are achieved for the 0.2 at% Cu-intercalated sample, which are more promising than those of many state-of-the-art n-type PbTe-based materials in the same temperature range. Based on our findings, we further propose criteria to select proper dopants exhibiting the dynamic doping effect, which is of fundamental importance for optimizing the electrical-transport properties.

Results and discussion

Powder X-ray diffraction (XRD) patterns reveal that all of the Cu-intercalated PbTe samples crystallize in the cubic rock-salt structure with the $Fm\bar{3}m$ space group and no obvious impurities are observed (see **Fig. S1** in the Supporting Information). Due to the tiny amount of Cu, no detectable change in the lattice parameters of our samples can be observed by XRD analysis. The microstructure and sample composition have also been characterized by transmission electron microscopy (TEM). For our samples with a trace amount of Cu (0-0.6 at%), neither excess elemental Cu nor a Cu-rich second phase was observed. However, the dynamic doping effect exhibited by the Cu-containing samples (see the detailed discussion below) indicates clearly that there should be excess Cu (not in solution) in these samples at room temperature. Consequently, it is likely that the dilute concentration of Cu is below the detection threshold of the characterization techniques. Thus, a control sample with 10 at% Cu was prepared using the same method under the same conditions as the other samples in the present work, and analyzed by TEM to confirm the existence of Cu-related secondary phases. As shown in **Fig. S2**, both Cu_2Te and elemental Cu were observed in this control sample (see also detailed discussion in the Supporting Information). Thus, we can conclude that the addition of Cu not only introduces interstitial Cu into the PbTe lattice but also results in excess Cu that is crucial for the dynamic doping effect.

As shown in **Fig. 1(a)**, an ultrahigh power factor was achieved for the Cu-intercalated n-type PbTe over the entire measured temperature range. Furthermore, the temperature-dependent power factor curve of our sample agrees well with the theoretically optimized curve (red solid line in Fig. 1(a)), indicating that the power factor of n-type PbTe can be fully

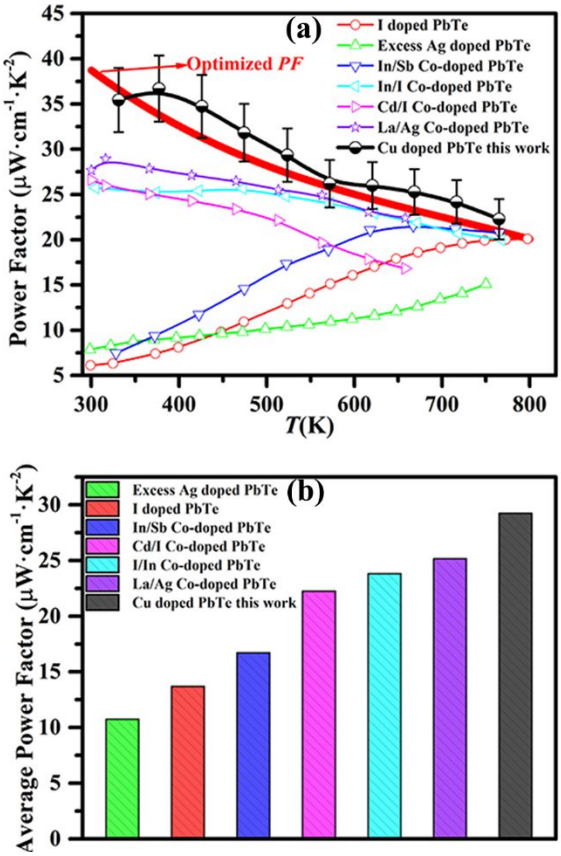

Fig. 1 Temperature-dependent power factor and average power factor for n-type PbTe. The solid lines with open shapes in (a) represent power factors reported in the literature for n-type PbTe samples with optimized doping compositions,[20-25] and the black solid line with half-filled circles represents the power factor of the sample with 0.2 at% Cu in this work (with the measurement error of 15%). (b) The average power factors of the samples plotted in (a) over their measured temperature ranges. The red solid line in (a) is the theoretical maximum power factor calculated by the single Kane band (SKB) model, assuming that the charge transport is dominated by the acoustic phonon scattering (see Supplementary Note 4 in the Supporting Information)

optimized over a large temperature range by incorporating Cu. It is also found from Fig. 1(a) that the power factor of the n-type PbTe is almost the same at high temperature (~20 μW cm^{-1} K^{-2} at 773 K), if an appropriate amount of dopant is added, independent of the elemental type of dopant. However, it is difficult to fully optimize power factor over a large temperature range by using a conventional dopant, because the carrier concentration remains nearly the same while the temperature varies. Our experimental results indicate that Cu can serve as an ideal dopant to achieve optimal carrier concentration for n-type PbTe over a large temperature range. Due to the optimized electrical-transport properties, the average power factor of our Cu-intercalated PbTe reaches a record value of ~29 μW cm^{-1} K^{-2} over the measured temperature range compared with those reported in the literature[20-25], almost three and two times larger than excess Ag-doped[23] and In/Sb co-doped PbTe[24], respectively (see **Fig. 1(b)**). The decrease in optimum power factor with increasing temperature can be understood by the increase in electron inertial effective mass.[22]

Cu-intercalated PbTe can exhibit an ultrahigh power factor over a wide temperature range because both its carrier concentration and mobility are fully optimized by the dynamic doping effect of interstitial Cu. As shown in **Fig. 2(a)**, the carrier concentrations of all of the Cu-containing samples show strongly temperature-dependent behavior. The carrier concentration increases rapidly with increasing temperature, which can be attributed to the dynamic doping effect due to the dissolving of Cu into the interstitial sites of the PbTe lattice with the increasing temperature. The carrier concentration then reaches a plateau at high temperature and remains almost the same with further increasing temperature, indicating that all the Cu atoms reserved in the second phase dissolve completely into the PbTe matrix. Additionally, the plateau shifts to higher temperature with increasing Cu content, indicating that the solubility of the interstitial Cu in PbTe increases with temperature. Due to the fast diffusion nature and small ionic radius of the Cu^+ cations, the formation energy of interstitial Cu in PbTe is much smaller than those of interstitial Pb and Ag. For instance, the formation energies of 0.2 at% interstitial Cu, Pb, and Ag in PbTe (derived by fitting the ascending part of the carrier concentration *vs* temperature curve;[16,23] see Fig. 2(a)) are 0.18 eV, 0.55 eV,[23] and 0.32 eV,[23] respectively. This indicates that the interstitial Cu is more effective as a dopant in optimizing the carrier concentration of PbTe than either Pb or Ag. The formation energy increases from 0.18 eV to 0.32 eV with the Cu content increasing from 0.2 at% to 0.6 at%, which can presumably be ascribed to the increased initial carrier concentration with the increasing Cu concentration.[26]

As shown in **Fig. 2(b)** and **(c)**, with the benefit of the dynamic doping effect, both the carrier concentration and mobility of n-type PbTe can be fully optimized over a wide temperature range, especially compared with the conventional doping system.[20,27] It has been reported that Ag also shows a similar dynamic doping effect in the PbTe matrix,[23] leading to an increased carrier concentration at elevated temperatures (see Fig. 2(b)). However, the carrier concentration and mobility of the excess Ag-doped PbTe sample are much less than the theoretically predicted optimal transport-property values (see dashed line in Fig. 2(b) and (c)), which could be ascribed to the following three reasons. First, for the carrier concentration, the ionic radius of Ag^+ (1.0 Å) is much larger than that of Cu^+ (0.6 Å), resulting in a much smaller room-temperature solubility of Ag^+

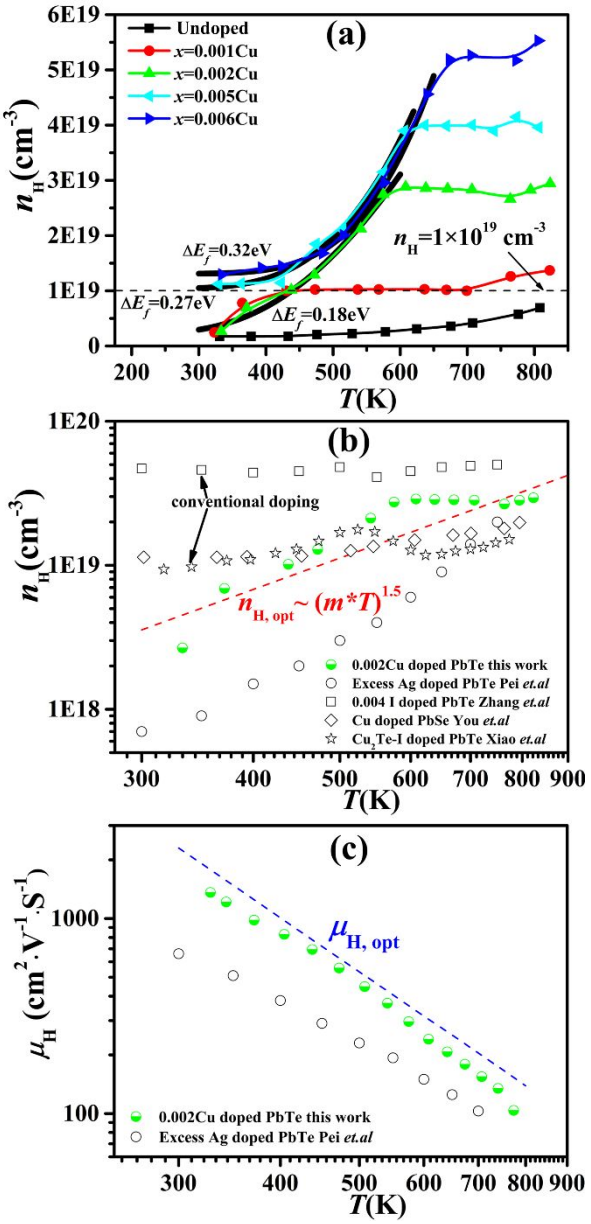

Fig. 2 (a) Temperature-dependent carrier-concentration values of $PbCu_xTe$ samples (x = 0, 0.001, 0.002, 0.005, and 0.006). The gray dashed line denotes the curve with the carrier concentration of 1×10^{19} cm^{-3}. The solid black lines are the fitting results for the ascending part of the carrier concentration *vs* temperature curve of the samples with x = 0.002, 0.005, and 0.006 using the exponential relationship of $e^{\Delta E_f/T}$, where ΔE_f is the obtained formation energy for the interstitial Cu. Temperature-dependent (b) carrier-concentration and (c) mobility values of the 0.2% Cu-doped PbTe. Results from the literature for I-doped PbTe,[20] Cu-doped PbSe,[19] Cu_2Te-I co doped PbTe,[27] and excess Ag-doped PbTe[23] are also included for comparison. The dashed lines in (b) and (c) represent the optimal carrier concentration and mobility, respectively, of Cu-intercalated PbTe.

in PbTe, in agreement with the formation energy shown above. Second, the diffusion speed of Cu in PbTe is much faster than that of Ag in PbTe.[28] Third, the large-size Ag_2Te precipitate embedded in the PbTe matrix leads to a remarkable reduction of the carrier mobility. Thus, interstitial Cu is more effective than Ag in optimizing the electrical-transport properties of n-type PbTe.

Compared to our recently reported Cu-PbSe system,[19] the Cu-intercalated PbTe almost achieves the ideal carrier concentration over the measured temperature range. On the other hand, the Cu-PbSe sample is overdoped at low temperature (see Fig. 2(b)). This can be well explained by their difference in the interstitial space. Lead chalcogenides have a face-centered cubic structure and Pb can be thought to fully occupy the octahedral interstices of the anion sublattice, so the interstitial dopant can only occupy the tetrahedral interstices of the anion sublattice.[29] Thus, we can conclude that the anion sublattice should be a determine factor for the degree of dynamic doping phenomenon. A concept of 'interstitial engineering' is thereby proposed, which is devoted to manipulating the interstitial space of the anion sublattice and achieving a nearly perfect dynamic doping effect. Taking the lead chalcogenide as an example, the size of the tetrahedral interstitial space is determined by the anion sublattice, and thus PbTe has the smallest tetrahedral interstitial space among the lead chalcogenides (see **Fig. S3** in the Supporting Information) because the ionic radius of Te^{2-} is the largest. The smaller interstitial space leads to the smaller solubility of Cu in the interstitial site of PbTe, ensuring a lower electron concentration in the low temperature range and a more predominant dynamic doping phenomenon, as compared with the previous reported Cu intercalated PbSe and PbS systems.[19] In detail, in the PbSe:Cu system, more Cu cations enter into the interstitial sites of the PbSe lattice at the same nominal doping level, resulting in the overdoping at low temperature (see Fig. 2(b)). Along the direction of 'interstitial engineering', it is found that the dynamic doping effect will vanish with increasing interstitial space. For example, in the Cu-intercalated $Bi_2Te_{2.7}Se_{0.3}$ system, the interstitial Cu tends to serve as a conventional n-type dopant, not a dynamic dopant, due to the large interstitial space between the interlayers.[30] Fortunately, the temperature-dependent solubility of interstitial Cu in PbTe satisfies the requirement for carrier-concentration optimization, leading to the nearly ideal carrier concentration for n-type PbTe (see Fig. 2(b)).

The strong temperature-dependent behavior of the carrier concentration and the corresponding electrical conductivity (**Fig. 3(a)**) can be well understood by the phase diagram of the PbTe-Cu pseudo-binary system (**Fig. 3(b)**). Since the onset temperature of the plateau in the carrier concentration curve denotes the ending temperature of the complete dissolution of Cu, the solid solubility limit of Cu in PbTe at this temperature is determined. Thus, we can construct a quasi-schematic phase diagram of the PbTe-Cu pseudo-binary system (Fig. 3(b)), and the solid line in Fig. 3(b) represents the the solvus line of the pseudo-binary PbTe-Cu system. For a given Cu concentration, Cu dissolves continuously into the PbTe matrix following the solvus line, leading to increased carrier concentration and electrical conductivity with increasing temperature. At a certain temperature, all of the Cu atoms completely dissolve into the PbTe matrix and the electrical conductivity reaches a maximum value. Thus, a peak appears on the temperature-dependent electrical-conductivity curve at this temperature, as shown in Fig. 3(a). The corresponding temperatures of the peaks (labeled by colored a, b, c, d, and e) can also be identified as the ending temperatures of the dissolution process, which can be perfectly superimposed on the solvus line in the phase diagram.

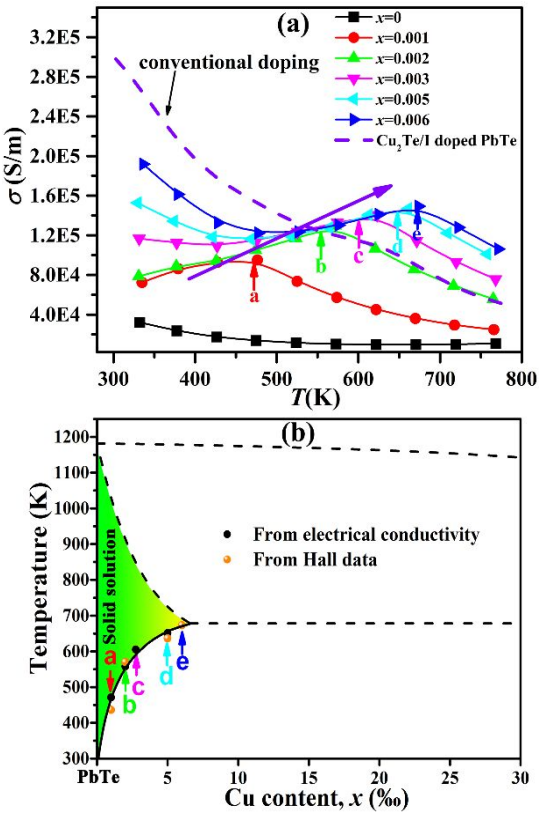

Fig. 3 (a) Temperature-dependent electrical-conductivity values of $PbCu_xTe$ samples (x=0, 0.001, 0.002, 0.003, 0.005, and 0.006). The dash line in (a) represents the electrical-conductivity of Cu_2Te-I co doped PbTe sample.[27] (b) Quasi-schematic phase diagram of the PbTe-Cu pseudo-binary system. The black dots denoted by a, b, c, d, and e correspond to the solid solubilities obtained from the peak temperatures of electrical-conductivity, and orange dots are the onset temperatures of the plateaus in the carrier concentration curve.

Extrinsic dopants are universally adopted to optimize the carrier concentration, but this may lead to modifications of the band structure and the carrier scattering mechanism.[31,32] According to a single-band model, in order to achieve a high carrier mobility at a given carrier concentration, the ideal dopant to regulate carrier concentration would have less influence on the band structure and the carrier scattering mechanism.[33] Thus, for optimization of the carrier concentration, both the extrinsic dopant itself and its occupied crystal sites should be carefully selected.

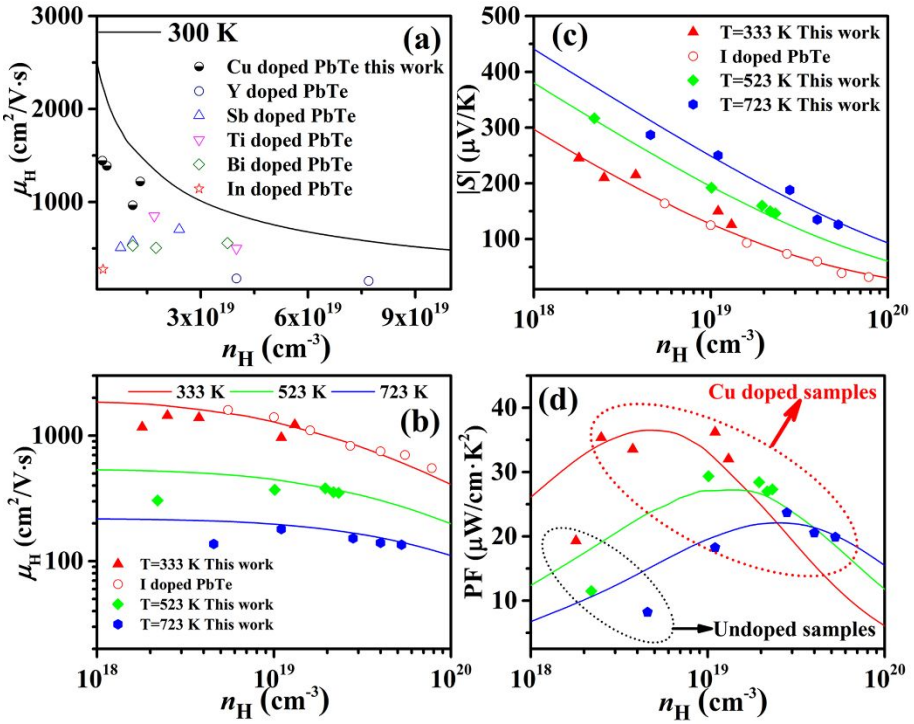

Fig. 4 Pisarenko relation of $PbCu_xTe$ samples at different temperatures. (a) Room-temperature Hall mobility as a function of carrier concentration. Carrier concentration-dependent (b) Hall-mobility, (c) Seebeck-coefficient (absolute value), and (d) power-factor values of the $PbCu_xTe$ (x = 0, 0.001, 0.002, 0.005, and 0.006) samples at different temperatures (333 K, 523 K, and 723 K). The half-filled and solid circles represent our experimental results in this work and the open symbols denote data reported in the literature.[22, 34-37] All of the solid lines in (a)-(d) are predicted by the SKB model (see Supplementary Note 4 in the Supporting Information).

For n-type PbTe, the conduction band could be disturbed by the substitution at the Pb site, leading to deteriorated carrier mobility.[16] As shown in **Fig. 4(a)**, the substitution of Bi,[33] Sb,[33] Y,[35] Ti,[36] or In[37] for Pb results in lower Hall mobility than that of the interstitial Cu-doped sample, which can be ascribed to the unchanged band structure of the Cu-intercalated PbTe samples. Experimentally, the Pisarenko relation is powerful in characterizing the band structure and the carrier-scattering mechanism.[38] As shown in **Fig. 4(b)** and **(c)**, both the Hall-mobility and Seebeck-coefficient values of our Cu-doped PbTe samples lie almost within the Pisarenko line, similar to I-doped PbTe.[22] This indicates that the interstitial Cu has little effect on both the conduction band and the carrier-scattering mechanism (acoustic phonons dominate the charge transport). As compared with the undoped sample, the carrier mobility of the Cu-containing sample is slightly enhanced, which is in agreement with a recent report in the literature[27] (the carrier-scattering mechanism can also be analyzed by the temperature-dependent carrier mobility; also see **Fig. S4** and detailed discussion in **Supplementary Note 3** in the Supporting Information).

According to the Pisarenko lines shown in Fig. 4(b) and (c), neither the band structure nor the carrier-scattering mechanism are changed, despite the fact that the fast-diffused Cu atom may show a liquid-like behavior that has also been observed in the high-temperature phases of Cu_2Se and Cu_2S, in which the electrical-transport properties are not altered by the Cu sublattice.[39] The electronic band structures of both pristine PbTe and Cu-intercalated PbTe have been theoretically calculated (see **Fig. S5** in the Supporting Information). The interstitial Cu does not change the band structure of PbTe but only shifts the Fermi level up to the conduction band, further confirming the electron-donor nature of the interstitial Cu. Our analysis discussed above reveals that the carrier concentration of n-type PbTe can be effectively and safely optimized by the interstitial Cu. As a result, the power factor of our Cu-containing samples fits well with the theoretically predicted value (see **Fig. 4(d)**).

Temperature-dependent electrical-transport properties are illustrated in **Fig. 5(a)-(c)**. As shown in Fig. 5(a), the Seebeck coefficient values are negative, indicating the n-type conduction behavior of all of the samples. With increasing Cu content, the room-temperature Seebeck coefficient decreases substantially because the carrier concentration increases with the intercalation of interstitial Cu, which is consistent with our carrier-concentration measurements (see Fig. 2(a)). For the Cu-free sample, the absolute value of the Seebeck coefficient starts to decrease and the electrical conductivity starts to increase above ~550 K because of intrinsic excitation. However, for the Cu-intercalated samples, both the temperature-dependent Seebeck-coefficient and electrical-conductivity values show broad peaks (see Fig. 5(b)), and the peaks shift to higher temperature with the increasing Cu content. This also differs from the conventional heavily doped degenerate

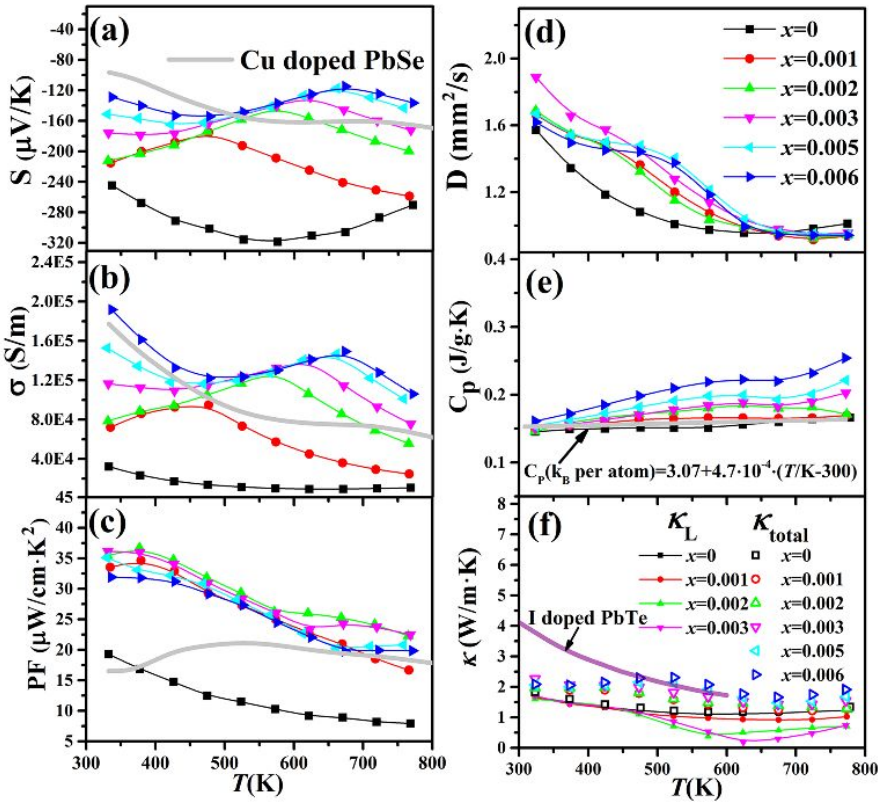

Fig. 5 Temperature-dependent thermoelectric-transport properties of $PbCu_xTe$ samples. (a) Seebeck coefficient, (b) electrical conductivity, (c) power factor, (d) thermal diffusivity, (e) specific heat, and (f) thermal conductivity. The gray solid lines in (a)-(c) are taken from Cu- intercalated PbSe.[19] The gray solid line in (e) represents the theoretical C_p of the pristine PbTe[22] and purple line in (f) represents the total thermal conductivity of I-doped PbTe taken from the literature.[22] The open and solid symbols in (f) denote the total and lattice thermal conductivities of $PbCu_xTe$ samples, respectively. The lattice thermal conductivity is calculated by subtracting $\kappa_E = L\sigma T$ from κ_{total}, where L is the Lorenz number obtained from the SKB model, σ is the electrical conductivity, and T is the absolute temperature.

semiconductor, but it is similar to the Cu-intercalated PbSe.[19] Therefore, the abnormal increase of electrical conductivity and decrease of Seebeck coefficient (absolute value) can be attributed to the dynamic doping effect of interstitial Cu, which is consistent with our temperature-dependent Hall measurement. Moreover, the electrical-transport properties, especially the power factor at low temperatures (see Fig. 5(c)), further confirm that the interstitial Cu shows a more prominent dynamic doping effect in PbTe than in PbSe. As a result, much higher power factor values, especially in the low-temperature range, are achieved in Cu-intercalated PbTe due to the significant dynamic doping effect.

Temperature-dependent thermal-transport properties of $PbCu_xTe$ samples are illustrated in **Fig. 5(d)-(f)**. The thermal diffusivity of the sample free of Cu, as shown in Fig. 5(d), is quite normal, and the slight increase of its thermal diffusivity at high temperatures can be ascribed to the increase of its electrical conductivity due to the bipolar effect. However, the Cu-containing samples show a broad bump which becomes increasingly more prominent with increasing Cu content. These broad bumps in the temperature-dependent thermal-diffusivity curves are the result of the complexities associated with the temperature-dependent solubility of interstitial Cu cations into the PbTe lattice, which is consistent with the temperature-dependent electrical-conductivity values.

The thermal-transport properties of Cu-intercalated PbTe samples are largely similar to those of Cu-containing PbSe samples, which can be well explained by the incorporation of Cu.[19] However, as shown in **Fig. 5(e)**, the specific heat C_p of the Cu-intercalated PbTe deviates significantly from the theoretical value at high temperatures, while the C_p of the Cu-intercalated PbSe remains consistent with the theoretical value. The C_p of the Cu-free PbTe sample, and that of samples doped with a tiny amount of Cu ($x = 0.001$), agrees well with the theoretical curve. However, for the samples containing more Cu, the specific heat starts to increase with both the Cu content and temperature, and this deviation from the theoretical value becomes increasingly more significant with the increasing Cu content. For instance, at 773 K, the C_p value of the $PbCu_{0.006}Te$ sample is 44% larger than that of the Cu-free sample. The increase of the C_p can be ascribed to the temperature-dependent solubility and the associated enthalpy in dissolving the Cu into the PbTe lattice, similar to the superionic phase transition in $Cu_{2-x}Se$.[40,41] For the Cu-containing PbSe, as we have discussed above, the solubility of Cu in PbSe is larger than that in PbTe at room temperature, leading to the fact that most of the Cu is dissolved into the PbSe lattice at room temperature, and thus the increase of its C_p is not as pronounced as that of the Cu-intercalated PbTe samples. Nevertheless, because the temperature-dependent solubility of Cu significantly impacts

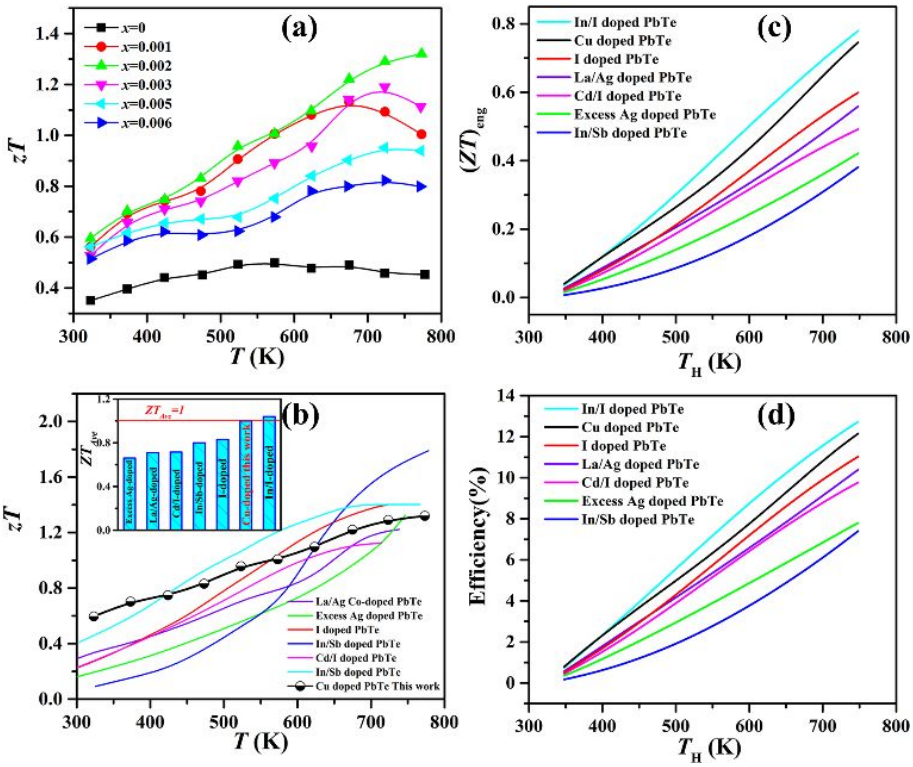

Fig. 6 Thermoelectric figure of merit *zT* for $PbCu_xTe$ samples. (a) Temperature dependence of the *zT* values for $PbCu_xTe$ (x = 0, 0.001, 0.002, 0.003, 0.005, and 0.006) samples. (b) Comparison of temperature-dependent *zT* values among the reported data. The inset shows the average *ZT* values of compositions plotted in (b), calculated by the integration method over the measured temperature range. (c) Comparison of hot-side temperature-dependent $(ZT)_{eng}$ values among reported compositions. (d) Calculated hot-side temperature-dependent leg efficiency values of n-type PbTe with different dopants. Calculation details for $(ZT)_{eng}$ and leg efficiency can be found elsewhere.[44]

the thermal diffusivity, it is necessary to use a heat capacity that includes the latent-heat contribution (*e.g.*, measured) to calculate the thermal conductivity.

The dynamic behavior of Cu (from both diffusion and dissolving) results in not only increased carrier concentration and C_p but also an apparent reduction in lattice thermal conductivity, especially for the samples with higher Cu content. Thus, as shown in Fig. 5(f), abnormal plateaus are observed in the temperature-dependent total thermal-conductivity curves due to the complexity in the dynamic behavior of Cu. A lattice thermal conductivity κ_L as low as 0.2 W m^{-1} K^{-1} at 623 K is determined for the sample with x= 0.003, which is even smaller than the glass-like κ_L of ~0.32 W m^{-1} K^{-1} calculated from the Cahill's model.[42] To explain this dramatically decreased κ_L, a diffusion (as opposed to phonon) -dominated thermal conductivity can be used. Such a model predicts a κ_L 37% lower than that calculated by Cahill's model,[43] resulting in a κ_L of ~0.21 W m^{-1} K^{-1} for PbTe. This diffusion-model result is very close to our experimental κ_L, indicating that the character of the atomic vibrations may be more diffusion-like in the Cu-intercalated PbTe.

Due to the enhanced electrical-transport properties and reduced lattice thermal conductivity, the Cu-intercalated PbTe samples show much higher *zT* values than the Cu-free sample over the entire measured temperature range, as shown in **Fig. 6(a)**. A peak *zT* of ~1.3 at 773 K and an average *ZT* of about 1.0 are obtained for the sample containing 0.2 at% Cu, which are higher than those of most of the state-of-the-art n-type PbTe materials (see **Fig. 6(b)** and its inset). In order to obtain a precise prediction of the conversion efficiency, the engineering figure of merit $(ZT)_{eng}$ as a function of the hot-side temperature (T_H) has also been calculated by fixing the cold-side temperature (T_C) at 323 K.[44] As illustrated in **Fig. 6(c)** and **(d)**, the calculated $(ZT)_{eng}$ is ~ 0.75 and the corresponding leg efficiency is about 12% at T_H = 748 K for our 0.2 at% Cu-intercalated PbTe sample, which is 47% higher than that of excess Ag-doped PbTe. Furthermore, the Cu-intercalated PbTe samples show good reproducibility for both electrical- and thermal-transport properties (see **Fig. S6** and **S7** in the Supporting Information). The sample also exhibits the same thermoelectric properties even after it has been left in ambient for 5 months at room temperature (see the third and fourth measurements of the thermoelectric-transport properties in Fig. S6 and S7 in the Supporting Information), indicating the high stability of the Cu-intercalated PbTe samples. In order to confirm the uniformity of our sample under a temperature gradient, we have characterized the Seebeck coefficient distribution of the $PbTeCu_{0.002}$ sample after 4 rounds of cycling ZEM measurements using the potential-Seebeck microprobe (PSM II). According to the mapping results (see **Fig. S8** in the supporting information), the Seebeck coefficient of the

repeatedly measured sample is uniform from the hot side to the cold side. This means that the Cu atoms do not migrate along the temperature gradient applied during the measurement. In addition, the Seebeck coefficient measured by the PSM is in the range from -230 μV/K to -260 μV/K, agreeing well with the value measured by ZEM near room temperature. Besides, the mechanical properties of our samples have been examined by the Vickers hardness test. The results (**Fig. S9**) show that the Vickers hardness of undoped PbTe sample is about 39.8 HV. The standard deviations of the measured results for all our specimens are within 4%, suggesting the uniformity of our samples. Compared to the pristine PbTe, a slight enhancement in the Vickers hardness is detected for the sample with 0.2 at% Cu, which can be attributed to the presence of interstitial Cu. More importantly, the mechanical properties of the sample do not deteriorate after two thermal shocks, further demonstrating its high stability in our experimental conditions. Nevertheless, it should be noted that the current conclusion for the stability cannot rule out the migration of copper ions in the real service environment of power generation, since the temperature difference (about 300 K) in the service environment is far greater than that in our experimental conditions (< 10 K). Thus, in order to utilize dynamic doping effect to enhance the performance of the advanced thermoelectric devices, much effort should be focused on the suppression of the atom motion under the large temperature gradient.

Based on our findings, we propose a set of criteria to exhibit the dynamic doping effect: 1) the extrinsic dopant shall have a proper atomic/ionic size because the temperature-dependent solubility of the extrinsic dopant must meet the requirement for carrier-concentration optimization for a given material; and 2) the extrinsic dopant and its dynamic behavior shall have little influence on both the electronic band structure and the carrier-scattering mechanism, which enables higher carrier mobility at a given carrier concentration. Thus, we propose another two cations (Li^+, Zn^{2+}) that may also serve as effective dynamic dopants for n-type PbTe because of their small ionic size and occupation at the interstitial site. Further studies on the Li^+-doped lead chalcogenide are in progress.

Conclusions

In summary, the intercalation of Cu into the PbTe lattice resulted in an effective dynamic doping effect. Optimized power factor close to the theoretical optimal value was achieved over the entire measured temperature range because the temperature-dependent solubility of interstitial Cu in PbTe satisfies the requirement for carrier-concentration optimization. Moreover, Cu intercalated in the PbTe lattice significantly reduced lattice thermal conductivity to the diffusion-mediated limit of thermal transport. As a result, a satisfactory peak zT of 1.3 and a fairly high conversion leg efficiency ~12% have been achieved for the PbTe sample with 0.2 at% Cu. Our experimental results demonstrated that the thermoelectric properties of n-type PbTe are effectively optimized by intercalated Cu acting as a dynamic doping element and suggest criteria for further selection of proper dopants exhibiting the dynamic doping effect.

Experimental

Synthesis:

Polycrystalline PbCuxTe (x = 0, 0.001, 0.002, 0.003, 0.005, and 0.006) samples were synthesized by melting high quality (>99.99%) Pb shots, Te chunks, and Cu pieces. The raw materials were weighed and loaded into silica tubes inside an Ar-filled glove box, and then sealed under vacuum. In order to clarify the microstructures of the PbTe-Cu systems, two samples with higher Cu content (x = 0.05 and 0.1) were also synthesized by the same method and under the same conditions as the other samples in this work (the thermoelectric-transport properties of these two samples were measured, as shown in **Fig. S10** in the Supporting Information). A small amount of excess Pb was intentionally added during the synthesis process to ensure that all of the samples showed the n-type conduction; such addition has been widely used in synthesizing n-type PbTe-based materials.[45] The silica tubes were heated to 1383 K over 10 h, held at this temperature for 16 h, and then quenched in cold water. The obtained ingots were ground into fine powders using an agate mortar and pestle. High-density (>97% of theoretical density) pellets with diameters of 10 mm (for thermal-transport measurement) and 15 mm (for electrical-transport measurement with size of about 2 mm × 3 mm × 15 mm) were densified by vacuum hot pressing at 823 K for 15 min under a uniaxial pressure of 65 MPa.

Characterization:

Powder XRD data were collected from the fine powders for all samples by a Rigaku D/max-2200 diffractometer with Cu Ka radiation at room temperature. The microstructures of the samples were characterized by transmission electron microscopy (TEM) using a JEM F200. Bright field (BF) and high-angle annular dark field (HAADF) imaging was performed in the STEM mode on all samples. Energy-dispersive X-ray spectroscopy (EDS) was used to determine the sample compositions. TEM specimens were prepared by mechanical slicing, polishing, and dimpling, followed by ion-milling with liquid nitrogen. Seebeck coefficient distribution of 0.2 at% Cu-intercalated PbTe sample was characterized by a potential-Seebeck microprobe (PSM II, Panco Ltd., Germany). Vickers hardness tests were carried out on an HXD-1000TM/LCD microhardness tester (Shanghai Taiming Optical Instrument), at a 0.098 N (10 gf) load with a 10 s loading time. The hardness is obtained by averaging 10 measurements for each sample.

Transport property measurements and band structure calculation:

The temperature dependence of the electrical-transport properties including Seebeck coefficient and resistivity were obtained in a ZEM-3 system (ULVAC-RIKO, Japan) under the protection of helium gas. The thermal diffusivity (a) values of the samples were measured using a laser flash apparatus with the Cowan model plus pulse correction (LFA 457, Netzsch). The total thermal conductivity was calculated via $k_{tot} = C_p \times D \times a$,

where C_p is the heat capacity, D is the actual density, and a is the thermal diffusivity of the sample. The density of the hot-pressed sample was measured by the Archimedes method, and the heat capacity (C_p) was measured by a differential scanning calorimetry thermal analyzer (DSC 214, Netzsch) at a heating rate of 10 K min^{-1}. The uncertainties of the resistivity, Seebeck coefficient, and total thermal conductivity data were estimated to be 5%, 5%, and 10%, respectively. Temperature-dependent Hall-coefficient measurements of the samples were obtained by using a four-probe Van der Pauw technique under a reversible magnetic field of 1.5 T under the protection of helium gas. The first-principles calculations on the band structure were the same as in our previous study.[19]

Conflicts of interest

There are no conflicts to declare

Acknowledgements

This work was supported by National Key Research and Development Program of China (Nos. 2018YFA0702100 and 2018YFB0703600), the National Natural Science Foundation of China (Grant Nos. 51772186, 51632005, and 51371194), the Science and Technology Commission of Shanghai Municipality (Grant No. 16DZ2260601); and the work done at the University of Houston was supported by the U.S. Department of Energy under contract DE-SC0010831. We thank Prof. J. H. Yang at the University of Washington for the fruitful discussion. J.L. designed the experiments. L.Y. and J.Z. carried out the experiments including sample preparation and thermoelectric-properties measurement. S.P. measured the heat capacity. Y.J. and K.W. contributed to TEM characterization. J.Y. and W.Z. calculated the band structure. Y.P. carried out high-temperature Hall measurement. Q.Z. calculated the $(ZT)_{eng}$ and the conversion efficiency. M.T.A. and G.J.S. analyzed the thermal-transport properties. J.L., J.Z., L.Y., Z.R., and W.Z. analyzed the experimental data systematically. J.L., L.Y. and J.Z. wrote the manuscript with input from all authors.

Notes and references

1 J. He and T. M. Tritt, *Science*, 2017, **357**, eaak9997.
2 S. W. Song, J. Mao, M. Bordelon, R. He, Y. M. Wang, J. Shuai, J. Y. Sun, X. B. Lei, Z. S. Ren, S. Chen, S. Wilson, K. Nielsch, Q. Y. Zhang and Z. F. Ren, *Mater. Today Phys.*, 2019, **8**, 25-33.
3 J. Mao, Z. Liu, J. Zhou, H. Zhu, Q. Zhang, G. Chen and Z. Ren, *Adv. Phys.*, 2018, **67**, 69-147.
4 C. Chang and L. D. Zhao, *Mater. Today Phys.*, 2018, **4**, 50-57.
5 Z. W. Chen, X. Y. Zhang and Y. Z. Pei, *Adv. Mater.*, 2018, **30**, 1705617.
6 L. D. Zhao, H. J. Wu, S. Q. Hao, C. I. Wu, X. Y. Zhou, K. Biswas, J. Q. He, T. P. Hogan, C. Uher, C. Wolverton, V. P. Dravid and M. G. Kanatzidis, *Energy Environ. Sci.*, 2013, **6**, 3346-3355.
7 K. Biswas, J. Q. He, I. D. Blum, C. I. Wu, T. P. Hogan, D. N. Seidman, V. P. Dravid and M. G. Kanatzidis, *Nature*, 2012, **489**, 414-418.
8 L. D. Zhao, S. Q. Hao, S. H. Lo, C. I. Wu, X. Y. Zhou, Y. Lee, H. Li, K. Biswas, T. P. Hogan, C. Uher, C. Wolverton, V. P. Dravid and M. G. Kanatzidis, *J. Am. Chem. Soc.*, 2013, **135**, 7364-7370.
9 B. Poudel, Q. Hao, Y. Ma, Y. C. Lan, A. Minnich, B. Yu, X. A. Yan, D. Z. Wang, A. Muto, D. Vashaee, X. Y. Chen, J. M. Liu, M. S. Dresselhaus, G. Chen and Z. F. Ren, *Science*, 2008, **320**, 634-638.
10 H. Wang, A. D. LaLonde, Y. Z. Pei and G. J. Snyder, *Adv. Funct. Mater.*, 2013, **23**, 1586-1596.
11 Y. Z. Pei, L. L. Zheng, W. Li, S. Q. Lin, Z. W. Chen, Y. Y. Wang, X. F. Xu, H. L. Yu, Y. Chen and B. H. Ge, *Adv. Electron. Mater.*, 2016, **2**, 1600019.
12 Z. W. Chen, B. H. Ge, W. Li, S. Q. Lin, J. W. Shen, Y. J. Chang, R. Hanus, G. J. Snyder and Y. Z. Pei, *Nat. Commun.*, 2017, **8**, 13828.
13 J. Mao, J. L. Niedziela, Y. M. Wang, Y. Xia, B. H. Ge, Z. H. Liu, J. W. Zhou, Z. S. Ren, W. S. Liu, M. K. Y. Chan, G. Chen, O. Delaire, Q. Zhang and Z. F. Ren, *Nano Energy*, 2018, **48**, 189-196.
14 H. J. Wu, L. D. Zhao, F. S. Zheng, D. Wu, Y. L. Pei, X. Tong, M. G. Kanatzidis and J. Q. He, *Nat. Commun.*, 2014, **5**, 4515.
15 Y. Lee, S. H. Lo, J. Androulakis, C. I. Wu, L. D. Zhao, D. Y. Chung, T. P. Hogan, V. P. Dravid and M. G. Kanatzidis, *J. Am. Chem. Soc.*, 2013, **135**, 5152-5160.
16 Y. Z. Pei, Z. M. Gibbs, A. Gloskovskii, B. Balke, W. G. Zeier and G. J. Snyder, *Adv. Energy Mater.*, 2014, **4**, 1400486.
17 G. J. Tan, L. D. Zhao and M. G. Kanatzidis, *Chem. Rev.*, 2016, **116**, 12123-12149.
18 J. H. Chen, C. Jang, S. Adam, M. S. Fuhrer, E. D. Williams and M. Ishigami, *Nat. Phys.*, 2008, **4**, 377-381.
19 L. You, Y. F. Liu, X. Li, P. F. Nan, B. H. Ge, Y. Jiang, P. F. Luo, S. S. Pan, Y. Z. Pei, W. Q. Zhang, G. J. Snyder, J. Yang, J. Y. Zhang and J. Luo, *Energy Environ. Sci.*, 2018, **11**, 1848-1858.
20 Q. Zhang, Q. C. Song, X. Y. Wang, J. Y. Sun, Q. Zhu, K. Dahal, X. Lin, F. Cao, J. W. Zhou, S. Chen, G. Chen, J. Mao and Z. F. Ren, *Energy Environ. Sci.*, 2018, **11**, 933-940.
21 K. Ahn, M. K. Han, J. Q. He, J. Androulakis, S. Ballikaya, C. Uher, V. P. Dravid and M. G. Kanatzidis, *J. Am. Chem. Soc.*, 2010, **132**, 5227-5235.
22 Y. Z. Pei, A. D. LaLonde, H. Wang and G. J. Snyder, *Energy Environ. Sci.*, 2012, **5**, 7963-7969.
23 Y. Z. Pei, A. F. May and G. J. Snyder, *Adv. Energy Mater.*, 2011, **1**, 291-296.
24 J. Zhang, D. Wu, D. S. He, D. Feng, M. J. Yin, X. Y. Qin and J. Q. He, *Adv. Mater.*, 2017, **29**, 1703148.
25 K. Ahn, C. P. Li, C. Uher and M. G. Kanatzidis, *Chem. Mater.*, 2009, **21**, 1361-1367.
26 A. F. Kohan, G. Ceder, D. Morgan and C. G. Van de Walle, *Phys. Rev. B*, 2000, **61**, 15019-15027.
27 Y. Xiao, H. J. Wu, W. Li, M. J. Yin, Y. L. Pei, Y. Zhang, L. W. Fu, Y. X. Chen, S. J. Pennycook, L. Huang, J. He and L. D. Zhao, J. Am. Chem. Soc., 2017, 139, 18732-18738.
28 C. C. Li, F. Drymiotis, L. L. Liao, H. T. Hung, J. H. Ke, C. K. Liu, C. R. Kao and G. J. Snyder, *J. Mater. Chem. C*, 2015, **3**, 10590-10596.
29 C. Schneider, P. Schichtel, B. Mogwitz, M. Rohnke and J. Janek, *Solid State Ionics*, 2017, **303**, 119-125.
30 W. S. Liu, Q. Y. Zhang, Y. C. Lan, S. Chen, X. Yan, Q. Zhang, H. Wang, D. Z. Wang, G. Chen and Z. F. Ren, *Adv. Energy Mater.*, 2011, **1**, 577-587.
31 S. Lin, W. Li, Z. Bu, B. Gao, J. Li and Y. Pei, *Mater. Today Phys.*, 2018, **6**, 60-67.
32 Z. Liu, J. Mao, S. Peng, B. Zhou, W. Gao, J. Sui, Y. Pei and Z. Ren, *Mater. Today Phys.*, 2017, **2**, 54-61.
33 H. Wang, X. L. Cao, Y. Takagiwa and G. J. Snyder, *Mater. Horiz.*, 2015, **2**, 323-329.
34 G. J. Tan, C. C. Stoumpos, S. Wang, T. P. Bailey, L. D. Zhao, C. Uher and M. G. Kanatzidis, *Adv. Energy Mater.*, 2017, **7**, 1700099.

35 L. Ruan, J. Luo, H. Zhu, H. Zhao and J. Liang, *J. Electron. Mater.*, 2015, **44**, 3556-3562.
36 G. Komisarchik, D. Fuks and Y. Gelbstein, *J. Appl. Phys.*, 2016, **120**, 055104.
37 Q. Zhang, E. K. Chere, Y. Wang, H. S. Kim, R. He, F. Cao, K. Dahal, D. Broido, G. Chen and Z. Ren, *Nano Energy.*, 2016, **22**, 572-582.
38 Y. Wu, W. Li, A. Faghaninia, Z. Chen, J. Li, X. Zhang, B. Gao, S. Lin, B. Zhou, A. Jain and Y. Pei, *Mater. Today Phys.*, 2017, **3**, 127-136.
39 Y. Sun, L. Xi, J. Yang, L. Wu, X. Shi, L. Chen, J. Snyder, J. Yang and W. Zhang, *J. Mater. Chem. A*, 2017, **5**, 5098-5105.
40 D. Vasilevskiy, M. K. Keshavarz, J. M. Simard, R. A. Masut, S. Turenne and G. J. Snyder, *J. Electron. Mater.*, 2018, **47**, 3314-3319.
41 D. R. Brown, R. Heijl, K. A. Borup, B. B. Iversen, A. Palmqvist and G. J. Snyder, *Phys. Status. Solidi-R.*, 2016, **10**, 618-621.
42 H. Wang, E. Schechtel, Y. Z. Pei and G. J. Snyder, *Adv. Energy Mater.*, 2013, **3**, 488-495.
43 M. T. Agne, R. Hanus and G. J. Snyder, *Energy Environ. Sci.*, 2018, **11**, 609-616.
44 H. S. Kim, W. S. Liu, G. Chen, C. W. Chua and Z. F. Ren, *P. Natl. Acad. Sci. USA*, 2015, **112**, 8205-8210.
45 A. D. LaLonde, Y. Z. Pei and G. J. Snyder, *Energy Environ. Sci.*, 2011, **4**, 2090-2096.

A nearly perfect dynamic doping effect is realized in PbTe through Cu intercalation, resulting in fully optimized temperature-dependent electrical-transport properties.